Surface & Coatings Technology 476 (2024) 130260

Contents lists available at ScienceDirect

Surface & Coatings Technology

journal homepage: www.elsevier.com/locate/surfcoat

A comprehensive structural and electrochemical study on the performance of Mn-phosphate layers

Sheila Silva-Fernández, Belén Díaz *, Raúl Figueroa, X. Ramón Nóvoa *, Carmen Pérez

CINTECX, Universidade de Vigo, Encomat Group, 36310 Vigo, Spain

ARTICLE INFO

Keywords:
Mn-phosphate
Accelerator
Ultrasonic stirring
Corrosion resistance
Crystal size
Coating mass
Fe/Mn ratio

ABSTRACT

Several manganese phosphating routes, including the influence of immersion time (15 min. and 30 min.), addition of accelerators ($Ni(NO_3)_2$, 2 g/l), modification in the activation stage (increased concentration in the activator), and ultrasonic stirring, were used to obtain films with a variety of characteristics. This research uses the following common analytical methods for the phosphate characterisation: scanning electron microscopy (SEM) and electrochemical techniques (potentiodynamic polarisation and electrochemical impedance spectroscopy (EIS). Thus, modifications in the coating mass, covering efficiency, surface appearance, and chemical composition/structure could be determined. This study showed that accelerators induced the formation of thicker layers (up to 125 % bigger), whereas ultrasonic stirring assisted with reducing the crystal sizes and developing denser films (up to 50 % reduction in the i_{corr} values). The dry frictional tests showed that the wear behaviour depended on the phosphate thickness, crystal density, and film tortuosity. A fine-grained structure or a thick film contributed to an improved wear performance (near 80 % reduction in the coefficient of friction), but grains that are too fine along with an intricate structure worsened the behaviour under frictional forces.

1. Introduction

Phosphate coatings are conversion layers that offer numerous benefits when grown on metallic substrates. Phosphating is one of the most frequent pre-treatments in the automotive and cold-forming industries because it consists of a dense, uniform, hard, and well-adhered layer that provides advantages such as corrosion and wear resistance [1]. In addition, due to its simplicity and relatively low-cost, the phosphate technology has been successfully expanded to the Mg or Ti alloys, often used in the biomedical industry [2–5]. Another more recent application field refers to its potential for the development of energy storage devices [6,7]. Among the many types of phosphate coatings, this study focuses on manganese phosphate. Its growth process has been well established, and numerous parameters have been traditionally studied to promote the development of films with enhanced performance. Some of these parameters include phosphating time [8–11] or temperature [12], bath composition [9,11–15], and pre-treatment conditions [9,16].

The phosphate coatings are usually deposited by immersion, once the metal piece has been properly degreased, pickled, and rinsed. Most commonly, Mn-phosphating proceeds at high temperatures (80 °C to 95 °C) and, compared to other equivalent processes, a long time is required (15 min to 1 h). The precise phosphating operational conditions will determine the coating thickness, the crystals' size, and composition, and thus, its performance. The process is initiated with the dissolution of the substrate at the micro anodes and reduction of the H^+ cations from the added phosphoric acid at the micro cathodes [17]. The resulting local pH increase promotes the deposition of insoluble products such as $Mn_3(PO_4)_2$ or, most commonly, hureaulite $(Mn,Fe)_5H_2(PO_4)_4.4H_2O$ due to the presence of Fe^{2+} cations in the bath.

The bath is commonly modified by adding accelerators, which are substances that prevent H_2 bubble formation and increase the phosphating rate [1,18], and metallic nitrates are usually used for this purpose [4,5,12]. The chemical nature of the cation along with the precise amount of the nitrates incorporated into the phosphating solution have been shown to influence on the coating mass, corrosion performance, and crystal density. Zhang et al. performed an extensive research on the role of several sophisticated [19–21] and eco-friendly accelerators [22,23] that allowed obtaining larger masses along with an improved corrosion resistance as compared to a conventional treatment after the same immersion time. Some researchers have suggested incorporating other additives, such as sodium silicate [13], permanganate ions [14], or several alkalising agents [11], which allowed the development of a

* Corresponding authors.
E-mail addresses: belenchi@uvigo.gal (B. Díaz), rnovoa@uvigo.gal (X.R. Nóvoa).

https://doi.org/10.1016/j.surfcoat.2023.130260
Received 27 September 2023; Received in revised form 24 November 2023; Accepted 28 November 2023
Available online 5 December 2023

variety of phosphate qualities.

An alternative procedure to avoid the accumulation of hydrogen bubbles at the surface is to use a stirring bath, and in particular, ultrasonic induced vibration has been studied [18,24,25].This experimental procedure has allowed the development of coatings with enhanced corrosion resistance as well as crystal refinement. All the experimental strategies that have been proposed to enhance the performance of the Mn-phosphate layers are most frequently assessed using common analytical characterisation methods such as scanning electron microscopy (SEM), X-ray diffraction (XRD), or electrochemical techniques. Thus, differences in the phosphate structure (composition and formulation of the deposited film), surface appearance (crystals size and density), and covering efficiency, among other features, can be concluded.

Electrochemical impedance spectroscopy (EIS) is frequently used to study phosphate layers. The accuracy of this technique lies in the reasonable selection of the best equivalent model for experimental data modelling. Studies in the literature that are related to phosphating assume the development of a planar electrode-electrolyte interface, which is modelled with a parallel circuit that is composed of a resistor and a capacitor, as in [16] or [26]. Even when the basic corrosion properties can be defined, no further conclusions about the film structure or its phosphate characteristics can be determined. In a previous study, we proposed that the phosphate film can be considered to be a porous electrode where the transmission line model was successfully applied [27]. This approach considers two parallel conduction paths, the electronic conduction along the solid phase (the phosphate film) and the ionic conduction through the electrolyte inside the film pores, with faradaic responses at the phosphate-electrolyte and bare substrate-electrolyte interfaces. This new analytical methodology has allowed a comprehensive analysis of the phosphate film growth [27,28].

The current research aims to extensively examine the morphological and chemical changes, that play a role in film performance, once the phosphating conditions are modified, rather than a proposal of new paths for the Mn-phosphating development. This kind of information is not available in the literature, although it is of paramount importance in the rationalisation of the phosphating process. Thus, an exhaustive characterisation of the Mn-phosphate layers prepared with traditional experimental strategies and using common analytical methods has been performed.

2. Experimental

The samples were cut (approximately 2 cm in height) from a hot rolled steel rod (manufactured by ArcelorMittal and kindly supplied by Galcore S.L.) that was 10 mm diameter. The chemical composition (% in weight) is shown in Table 1. The samples were degreased at ambient temperature in 1 M NaOH for 5 min and etched at 50 ± 1 °C in 1.8 M H_2SO_4 for 20 min. After each cleaning step, samples were carefully rinsed with water. Before phosphating, there was an activation period of 2 min in a commercial product (Fixodine®M™) to promote the formation of a dense and homogeneous film. The phosphating temperature was fixed at 86 ± 1 °C. Phosphating time, the phosphating bath, and activation conditions were modified to produce coatings with a variety of qualities. The influence of the stirring was also included as a treatment variable. Stirring was performed by placing the phosphating beaker in a cleaning ultrasonic device that was set at 40 kHz and 120 W. The operating conditions used in this study are summarised in Table 2. The time for the quickest treatment was fixed to 15 min since no uniform coatings could be obtained for a shorter immersion period. A series of three samples were simultaneously treated in the same bath containing about 100 ml of solution. Once used, the solution was discarded, and a fresh solution was used for a new series of samples. After phosphating, samples were rinsed with water, dried in warm air, and kept in a desiccator before the characterisation analyses.

Table 2
Phosphating operational conditions used in this study.

Phosphate designation	Activation step	Bath	Ultrasonic stirring	Time
P15-P30	0.05 g/l	A	No	15–30 min
PU15-PU30	0.05 g/l	A	Yes	15–30 min
PB30	0.2 g/l	A	No	30 min
PN15-PN30	0.05 g/l	N	No	15–30 min
PNU15-PNU30	0.05 g/l	N	Yes	15–30 min

Bath A: H_3PO_4 21.8 g/l, $MnCO_3$ 11.8 g/l, HNO_3 5.3 g/l and H_2O_2 0.02 g/l [24]. Bath N: bath A + $Ni(NO_3)_2$ 2 g/l.

The coating weights were measured using the stripping method [1]. The phosphated pieces were immersed in a solution of 2.4 g of Sb_2O_3 (2 wt%) in 100 ml of HCl (37 %) for 5 min at ambient temperature. The weight loss, established as mass per unit area, was then computed.

A scanning electron microscope (SEM, JEOL® 5410, OXFORD®), equipped with an Energy Dispersive Spectrometer detector (a Link ISIS 300 EDS) was used for the structural and chemical characterisation. The whole surface of the images taken at x500 was considered for the EDS quantification.

The electrochemical analyses were completed with an AUTOLAB PGSTAT-204 (Metrohm AG, CH) using electrochemical impedance spectroscopy (EIS) and the linear sweep voltammetry (LSV) techniques. The three electrodes set-up was used with a graphite sheet and a Hg/Hg_2SO_4 electrode as counter and reference electrodes, respectively. The electrolyte was a 0.1 M Na_2SO_4 solution.

The EIS measurements were performed at the open circuit potential (OCP), after 30-min stabilization period, at a frequency range of 1 MHz-10 mHz, and with a potential amplitude of 10 mV rms. For the impedance data fitting, the equivalent circuit shown in Fig. 1 was used.

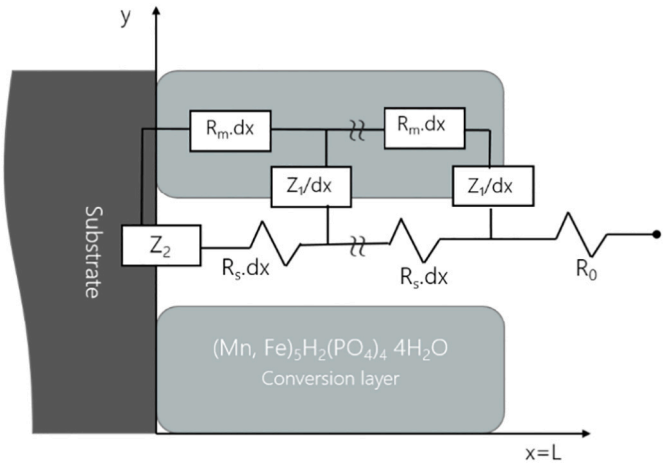

Fig. 1. Equivalent circuit used for the impedance data modelling.

Table 1
Chemical composition of the steel substrate (weight %).

C	Mn	Si	S	P	Cr	Ni	Mo	Cu	V	N	Fe
0.815	0.783	0.160	0.003	0.007	0.150	0.070	0.013	0.116	0.004	0.007	balance

Development of a porous electrode was considered, and the model was based on a transmission line (Eq. (1)). In the own phosphate film, several elements are repeated, with *dx* corresponding to a small portion of the film thickness and *L* to the total length of the pore. Some of these elements are representing the substrate (Z_2) and some of them are representing the porous electrode (R_m, R_s and Z_1). Z_2 is the impedance at the uncovered substrate/electrolyte interface, and the charge transfer resistance (R_2) and the double layer capacitance (C_2) are the related parameters. R_m is the response of the solid phase of the porous electrode, and it provides the '*apparent resistivity*' of the phosphate conversion layer. This value depends on the chemical structure of the own layer, and thus, on its own resistivity, as well as on the fraction of covered surface. It can be described as $\rho_m * \frac{S_t}{S_c}$, where ρ_m is the '*actual phosphate resistivity*', S_t is the total substrate area, both covered and uncovered, and S_c is the covered area. R_s represents the response of the electrolyte inside the pores, and similarly it provides an '*apparent resistivity*' defined as $\rho_s * \frac{S_t}{S_u}$, where ρ_s is the '*actual electrolyte resistivity*', S_t is the total substrate area, and S_u is the uncovered area. Z_1 corresponds to the interfacial impedance at the walls of the pores, which is composed of a charge transfer resistance and a double layer capacitance, arranged in parallel. R_0 shows the external electrolyte resistance, between the reference electrode and the outermost face of the phosphate film. The impedance function corresponding to the whole circuit is given in Eq. (1). Previous studies on porous conductive layers showed the suitability of this model [27–30]. The impedance spectra obtained for the bare substrate were fitted with a less complex model, which is composed uniquely of the resistance R_0 and the element Z_2 (the simplified Randles circuit) because the behaviour corresponded to that of a flat surface.

$$Z(\omega) = R_0 + \frac{R_m \bullet R_s}{R_m + R_s} \bullet L + \frac{\sqrt{\gamma}\left(2\,R_m\,R_s + \left(R_m^2 + R_s^2\right)cosh\left(L\sqrt{\gamma}\right)\right) + \delta R_s^2 sinh\left(L\sqrt{\gamma}\right)}{\sqrt{\gamma}(R_m + R_s)\left(\sqrt{\gamma}sinh\left(L\sqrt{\gamma}\right) + \delta cosh\left(L\sqrt{\gamma}\right)\right)} \text{ with } \gamma = \frac{R_m + R_s}{Z_1(w)}, \delta = \frac{R_m + R_s}{Z_2(w)}, Z_i(w) = \frac{R_i}{1 + (jwR_iC_i)^{\alpha_i}} \ (i = 1, 2) \tag{1}$$

For the LSV tests, a potential window ±150 mV vs. the OCP was chosen. The potential was swept at 1 mV/s. The corrosion current density values were computed using the Tafel analysis. These values provided an assessment of the coating efficiency so that at the lowest the values, the least amount the substrate remains exposed to the electrolyte.

A conventional pin-on-disk setup was used to validate the wear performance. A MT series tribometer (MICROTEST®) was used for the measurements. The pin was loaded with a force of 25 N that was applied in a direction that was normal to the samples. The tests were performed at a rotational speed of 0.03 m/s with a radius of 1.5 mm. The pin was a ball of AISI 52100 steel with 4 mm diameter. The tests were concluded after a sliding distance of 20 m was achieved. No lubricant was added. The coefficient of friction was recorded as a function of the sliding distance.

3. Results and discussion

The results corresponding to the layers that were tested will be presented and discussed separately according to the preparation conditions. The complete characterisation, including corrosion resistance, coating weight, structural/compositional analysis, and impedance spectroscopy, was included for each of the tested experimental variables (as described in Table 2). Finally, the results corresponding to the SEM cross-sectional analyses and the wear performance will be jointly discussed.

3.1. Bath A: influence of immersion time, ultrasonic stirring and activation stage

3.1.1. SEM/EDS characterisation

Fig. 2 shows the images that were taken with the SEM for the layers prepared in bath A. For the stagnant bath, no large differences were observed in the surface morphology when the treatment time increased from 15 to 30 min. Coarse crystals (average size approximately 50 μm) that were constituted as flat single sheets grown almost perpendicularly to the metal with a suitable degree of cover and a smooth and uniform surface appearance, were obtained after both immersion periods. The ultrasonic stirring caused a marked reduction in the crystal size, no matter the treatment time. Thus, the crystal surface density notably increased in the layers that were developed in the ultrasonically stirred bath, which is consistent with the results of other studies [24,25,31]. The vibration facilitates nucleation of the phosphate crystals due to the cavitation that was created, which generates local changes in temperature and pressure [18,24]. Ultrasound promoted the growth of crystals with a variety of sizes (mostly less than 5 μm in size for the shortest treatment; Fig. 2c). Slight crystal growth can be perceived after a longer stirring period (less than 10 μm in size; Fig. 2d). Ultrasonic stirring also induces the formation of prismatic-shaped crystals.

A possible explanation to the fact that the crystals are larger after 30 min with ultrasonic vibration could be connected to a competition in the film growing stage (Fig. 2c vs. d). Once the nuclei fully covered the surface, some crystals are more suitably disposed for their development and then grow preferentially. Such a phenomenon is not observed in case the nucleation is poorly assisted, as in the stagnant condition, where the number and size of crystals is essentially the same independently of time (Fig. 2a vs. b). This observation is in line with the obtained coating weights that will be exposed in the Section 3.1.2 (Table 3). No further development has been observed in the stagnant treatment after 15 min whereas a thicker layer was obtained when extending the stirring for 30 min.

Modification in the activation stage also promotes a noticeable decrease in crystal size (average size, 10 μm; Fig. 2e). The crystals are of uniform size. Increasing the activator concentration (denoted as 'PB') provides the arrangement of a higher number of sites for the phosphate crystals nucleation, which leads to the formation of a finer-grained structure [32–35].

The chemical composition (atomic %) for each layer is also shown in Fig. 2. The main elements, P, Mn, and Fe, have been considered. The P/(Mn + Fe) atomic ratio remained at approximately 0.8, which suggests the development of a layer that is essentially composed of hureaulite, $(Mn, Fe)_5H_2(PO_4)_4{\cdot}4H_2O$, which is the expected Fe—Mn mixed phosphate [1,8,13,14,36]. Some differences in the Mn/Fe ratio can be discerned. Thus, a slight Fe enrichment is detected for the film that was prepared in the stagnant bath after a longer phosphating time. A progressive increase in the Fe^{2+} content of the bath due to the longer phosphoric pickling action could have caused this change in composition.

However, the ultrasonically induced stirring helps with the development of a Mn-enriched hureaulite, and this occurs more markedly with the longer immersion period. Stirring seems to assist the transfer of the fresh bath solution near the metallic substrate. Thus, the Fe^{2+} ions that are generated due to the acid pickling do not stay in the region close to the electrolyte/substrate interface, which makes it more difficult to be incorporated to the growing phosphate layer.

A significant Fe enrichment was verified in the film that was developed after the change in the activation stage. Similar variations in the phosphate composition have also been found by other authors after modifications in the activator conditions [9,37]. The higher number of nucleation sites facilitates the incorporation of the Fe^{2+} ions, which are produced in the pickling reaction, to the phosphate structure. A slightly lower P/Mn + Fe ratio was also obtained, suggesting a modification in the type of the developed phosphate. Other likely products that possess a

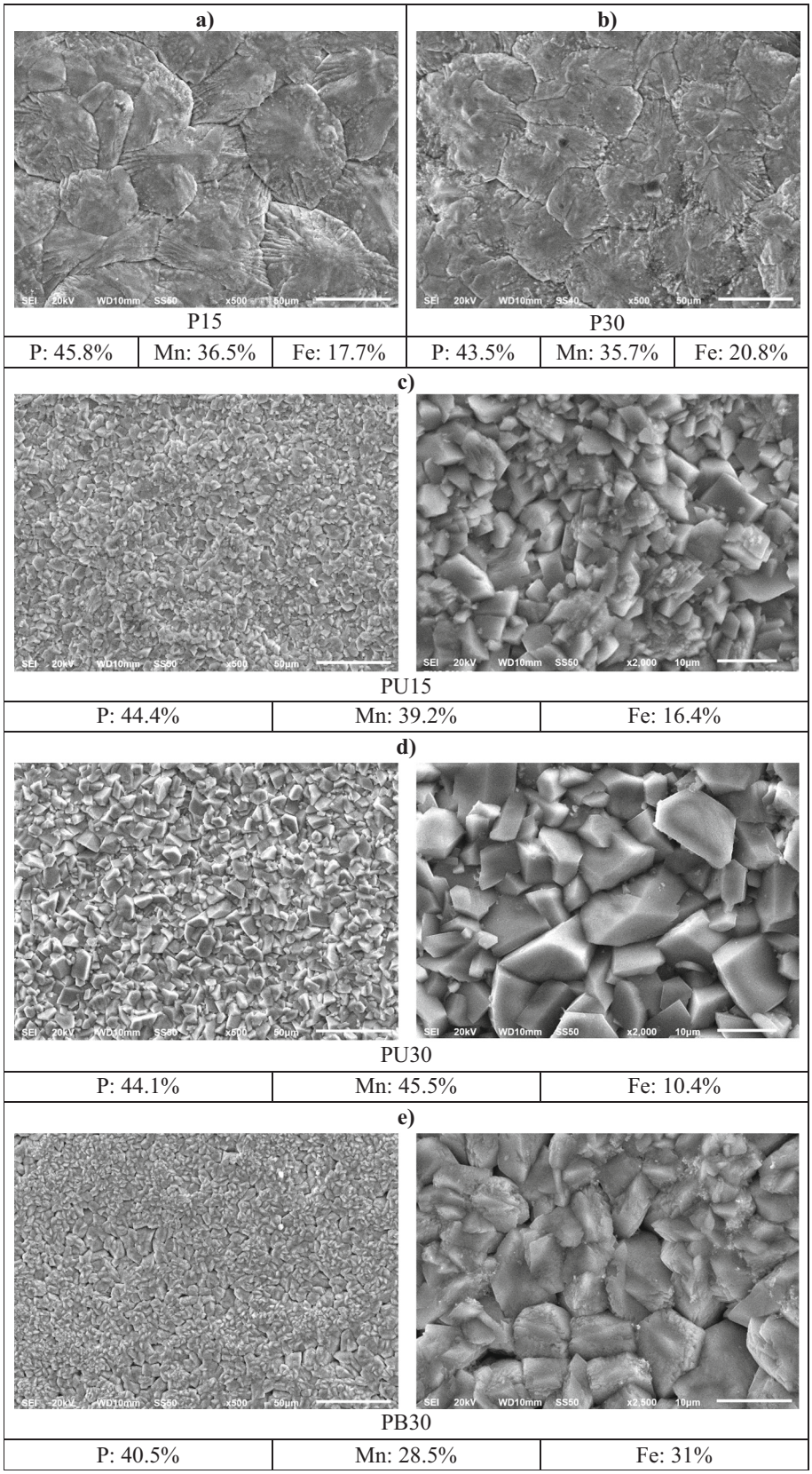

Fig. 2. SEM images for the phosphate films prepared in the original bath without stirring for a) 15 min and b) 30 min; under ultrasonic-induced stirring, for c) 15 min and d) 30 min; with variation in the activation bath (30 min of phosphating time); and with e) increased concentration of the activator. The chemical analysis as the atomic % is included.

Table 3
Results corresponding to coating weights and current densities for the layers obtained in bath A. (*see the experimental conditions in Table 2).

Sample*	Coating weight (g/m^2)	i_{corr} ($\mu A/cm^2$)	E_{corr} ($mV_{vs.\ Hg/HgSO4}$)
Bare substrate	–	6.79	−929
P15	16.1	1.01	−818
P30	17.3	2.33	−880
PU15	10.2	1.50	−763
PU30	18.1	1.12	−740
PB30	15.9	1.86	−820

reduced P/Mn + Fe ratio could be $MnFe_2(PO_4)_2.H_2O$ or $Mn_9Fe_2(PO_4)_8.14H_2O$ [8]. In addition to the reduction in the P/Mn + Fe ratio, the Fe/Mn ratio remained above 1; however, for the original activation solution (film P30), this ratio was lower. Enhanced activation then promotes both the formation of smaller crystals and Fe enrichment in the phosphate film.

3.1.2. Coating weight and polarisation curves

Table 3 includes the results corresponding to the coating weight for the phosphate layers that were grown in bath A. An increase in the phosphating immersion period lead to the growth of a thicker layer under both still and ultrasonically stirred conditions, which was more markedly for the latter state. The ultrasonic stirring generated a layer that was approximately 35 % thinner than that grown in the stagnant solution when the shortest immersion period was compared. These results were similar to those reported in other studies [24,25]. For the longer immersion processes, no great differences were obtained between the two preparation modes. This comparison suggests stabilization in the coating development after 15 min for the still condition, whereas in the stirred mode, the phosphate continues growing after that period. The local chemical conditions at the substrate/electrolyte interface may be refreshed due to the ultrasonic-induced stirring, which allows subsequent phosphate development. Conversely, in the stagnant bath, depletion seems to occur at the interfacial area, which hinders further film growth. A similar result was reported in relation to the combined influence of the two factors, time and ultrasonic stirring [24].

Increasing the concentration of the activation agent did not produce a great change in the coating weight (PB30 vs. P30). A reduction in the coating mass could be expected due to the enhanced activation, as concluded by Azhaarudeen et al. [38], but for a longer phosphating time, as discussed in this study, a reduction in the coating mass should not be expected.

Fig. 3 shows the polarisation curves measured in the 0.1 M Na_2SO_4 solution. The corrosion current density and corrosion potential values, which were determined using Tafel extrapolation, are also presented in Table 3. The current density values obtained for the phosphated pieces were lower than for the bare substrate, which agrees with the development of a physical barrier that at least partially hinders electrolyte accessibility to the metal. Thus, the observed differences are related to changes in the substrate area that remains exposed to the electrolyte. The more anodic corrosion potential values recorded for the coated specimens agree with a lowest corrosion susceptibility.

Immersion for 30 min produced an increase in the current density values compared to the shorter treatment of 15 min, which suggests the development of a more defective coating in terms of its covering efficiency. However, no significant differences were detected in morphology or mass, as shown above. A longer phosphating period, under the current experimental conditions, leads to longer exposure to the phosphoric acid solution so that more pronounced pickling occurred in those bare areas. Phosphating times greater than 15 min in the original bath caused dissolution of the substrate at the uncovered sites, but the coating masses indicated that the film showed no significant further development. At this stage, the dissolution of the substrate, due to the phosphoric acid etching, seems to be dominant over the formation of the coating [39]. Then a feasible explanation to the increased current density could be connected to a roughening effect produced due to the substrate dissolution at the uncoated sites. The prolonged acid pickling

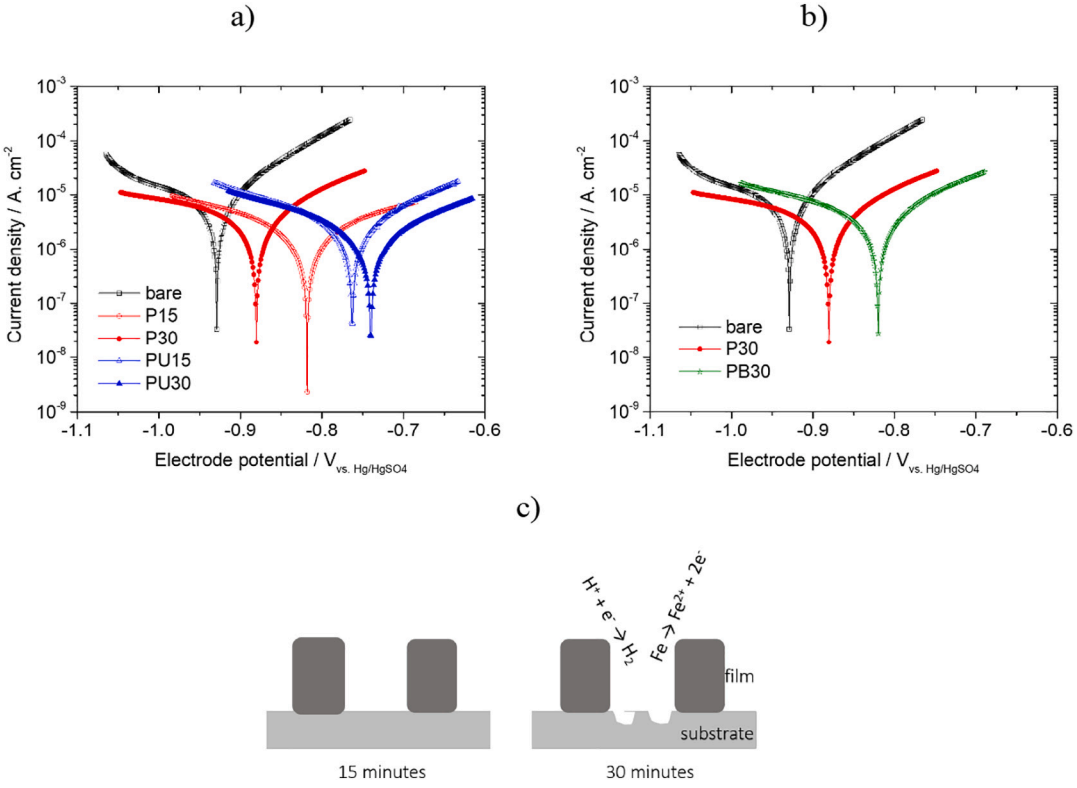

Fig. 3. Polarisation curves obtained for the phosphate films prepared in the original bath a) with and without ultrasonic stirring, b) with the modified activator, c) the scheme for developing of a rougher substrate during the longer phosphating time in the original bath.

leads to an increase in roughness and then in the active surface at the uncoated sites, which produces the observed increase in the current density values. A simplified sketch to visualise this discussion is presented in Fig. 3c. This suggestion also agrees with the increase in the Fe content for the layer that was developed after 30 min (Fig. 2b).

The ultrasonically stirred condition leads to a reduced coating efficiency with increased electrolyte access when the shorter periods were compared. However, the extended ultrasonic treatment led to the formation of a more compact film. A discussion about the precise effect of the ultrasonic vibration is not simple when previous studies are taken into consideration [25,31]. No clear conclusion can be stated in terms of the coating weight or the covering efficiency, which means that the modifications will depend on the phosphating conditions (i.e., temperature, time, and bath composition). In this study, increasing the immersion time and using ultrasound mainly assists the growth of crystals that were created, which leads to an improved covering and an increased coatings mass.

There were no large changes after the modifications in the activation stage, but the induced crystal refinement produces a slightly denser film. Comparing the films obtained after 30 min (P30, PU30, and PB30) showed a direct correlation between the crystals' density and the film compactness. Thus, a greater crystals density is associated with a denser phosphate film.

3.1.3. Electrochemical impedance spectroscopy analysis

Fig. 4 shows the Nyquist plots that correspond to the layers that were developed in the original bath. For all of the phosphated specimens, the impedance was greatly increased compared to the bare substrate, which indicates improved corrosion performance. The depressed shape of the Nyquist plots corresponded well to the distribution of the electric field it would occur in the transmission line in Fig. 1. According to the presented equivalent circuit (Fig. 1 and Eq. (1)), the low frequency limit does not correspond to the corrosion resistance, so a comprehensive analysis of all the parameters that are included in the model will be discussed. The fitted values are indicated in Table 4. The electrolyte resistance, R_0, is not presented because it is meaningless for the purpose of this study; an average value of 27.4 $\Omega.cm^2$ was obtained, which is consistent with the expected quantity for a 0.1 M Na_2SO_4 solution.

To proceed with the fitting, the thickness, L, of each film must be fixed because all the distributed parameters of the equivalent model depend on it. The values were taken from the coating masses, after dividing by the theoretical density value of a hureaulite-type compound (3.2 g/cm^3) [1].

The parameters related to the Z_2 time constant, R_2 and C_2, the charge transfer resistance, and the double layer capacitance at the electrolyte/uncoated substrate interface, were consistent with the trend that was obtained for the corrosion current densities (Table 3), which is an indication of the reliability of the fitted data. Thus, the highest R_2 and lowest C_2 were obtained for the sample coated with the film that was developed after the shorter period without stirring. However, the worst film (lowest R_2 and highest C_2) was obtained after immersion for 30 min in the same bath.

For Z_1, no large changes were obtained among the R_1 values, but the C_1 values differed significantly. The extension in the immersion period (P15 vs. P30) led to a significant reduction in the R_1C_1 time constant, from 812 ms to 7.8 ms. This suggests that there were changes in the interfacial response between the phosphate film and the electrolyte inside the pores, which were more rapidly developed for the coating that was obtained after 30 min. Such a change suggests the development of a more conductive film that facilitates that interaction. When the R_m values were compared, support for this idea was obtained. The R_m values depend on the precise coated area, which is unknown, but a higher coated area is expected for the P15, according to the greatest covering efficiency, which was already described (R_2 and C_2). The accurate R_m value (after correction by the true coated area) for this film would still be higher than the accurate R_m value of the P30 film. Thus, a more

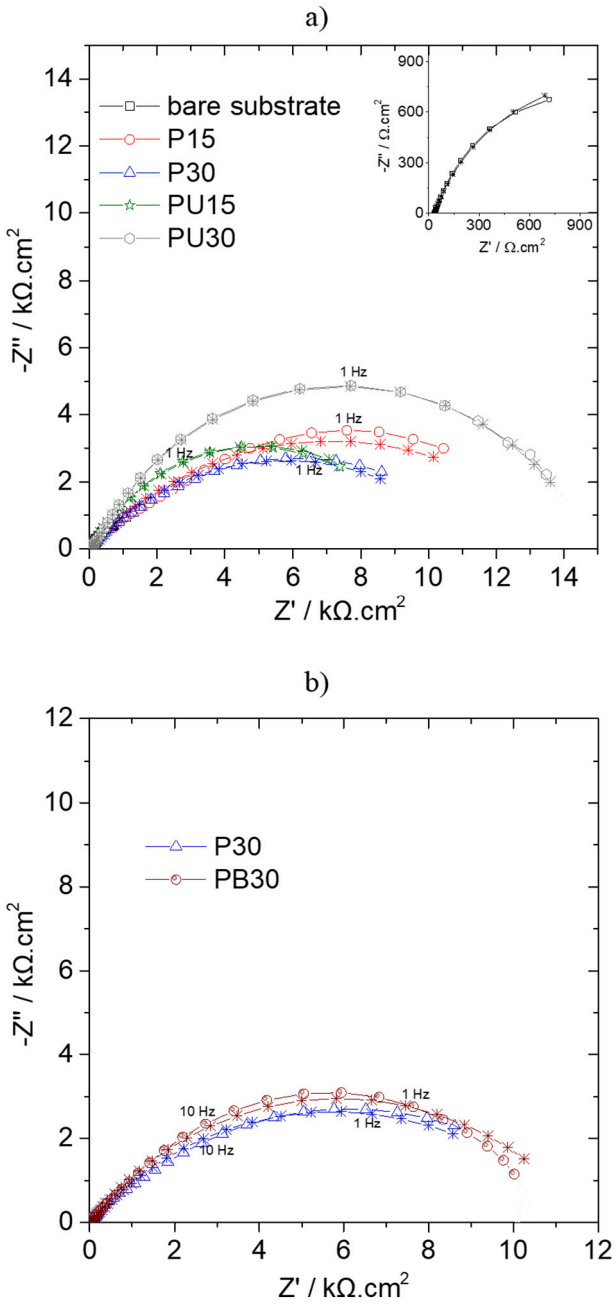

Fig. 4. Nyquist plots obtained in the 0.1 M Na_2SO_4 solution after development of the layers in bath A for a) stagnant and ultrasonically stirred baths and b) with the modified activation stage. The fitted data are represented by the stars.

Table 4
Fitting parameters of the phosphate layers prepared in bath A. The equivalent circuit that is presented in Fig. 1 was used for the fitting.

	R_m (kΩ. cm)	R_s (kΩ. cm)	R_1 (Ω. cm^3)	C_1 (mF. cm^{-3})	a_1	R_2 (kΩ. cm^2)	C_2 (μF. cm^{-2})	a_2
P15	5532.1	49.6	14.3	56.8	0.5	43.1	1.3	0.8
P30	1032.1	11.2	26.3	0.3	0.9	18.6	19.1	0.5
PU15	247.4	8.5	5.1	128.3	0.7	31.4	9.7	0.7
PU30	4851.6	31.7	13.8	4.6	0.8	36.3	4.9	0.7
PB30	173.6	7.2	9.4	1.1	0.7	31.2	10.1	0.6

conductive coating was grown during the longer immersion period in the stagnant bath.

The ultrasonic stirring minimally changed the Z_1 time constant for the layer growth after 15 min (compared to P15). The reduction obtained in the R_m seems to be related to changes in the coating structure rather than changes in the conduction ability. Thus, the structure that was developed with stirring (PU15), and containing smaller crystals, could create quicker electrical access to the substrate. Conversely, the electrical path to connect with the substrate may be more twisty for P15, causing an increased R_m value because the thickness values used for the fitting assume the development of a uniform columnar structure. This may not be the real state, and as a consequence, the R_m and R_s parameters will be modified when the direction of film growth is not uniform.

The increased immersion time in the stirred bath produces another reduction in the Z_1 time constant, suggesting similar changes in the conduction level, as mentioned above. However, the R_m value increased by one order of magnitude. The growth of a thicker layer after 30 min leads to the development of a longer twisty path to reach the substrate. Then, although the PU30 layer was intrinsically more conductive, its structure had a more complex path for electrical conduction. This is why the R_m value for the PU30 film was higher than that for the PU15. The mathematical correction in the R_m value, if the true length would be known, would lead to a lower value (resistance is inversely proportional to the length).

No important changes were identified in the conduction between both layers that were obtained after 30 min (P30 and PU30) because similar values for the Z_1 time constant were computed. The significant difference obtained in the R_m values suggested that there were changes in the coating structure. Thus, the observed modification is related to the production of a more tortuous film when the bath is ultrasonically stirred.

The modifications obtained in the R_s value validate the above discussion. The film that was prepared after 15 min in the stagnant bath was more compact and provided more limited accessibility of the

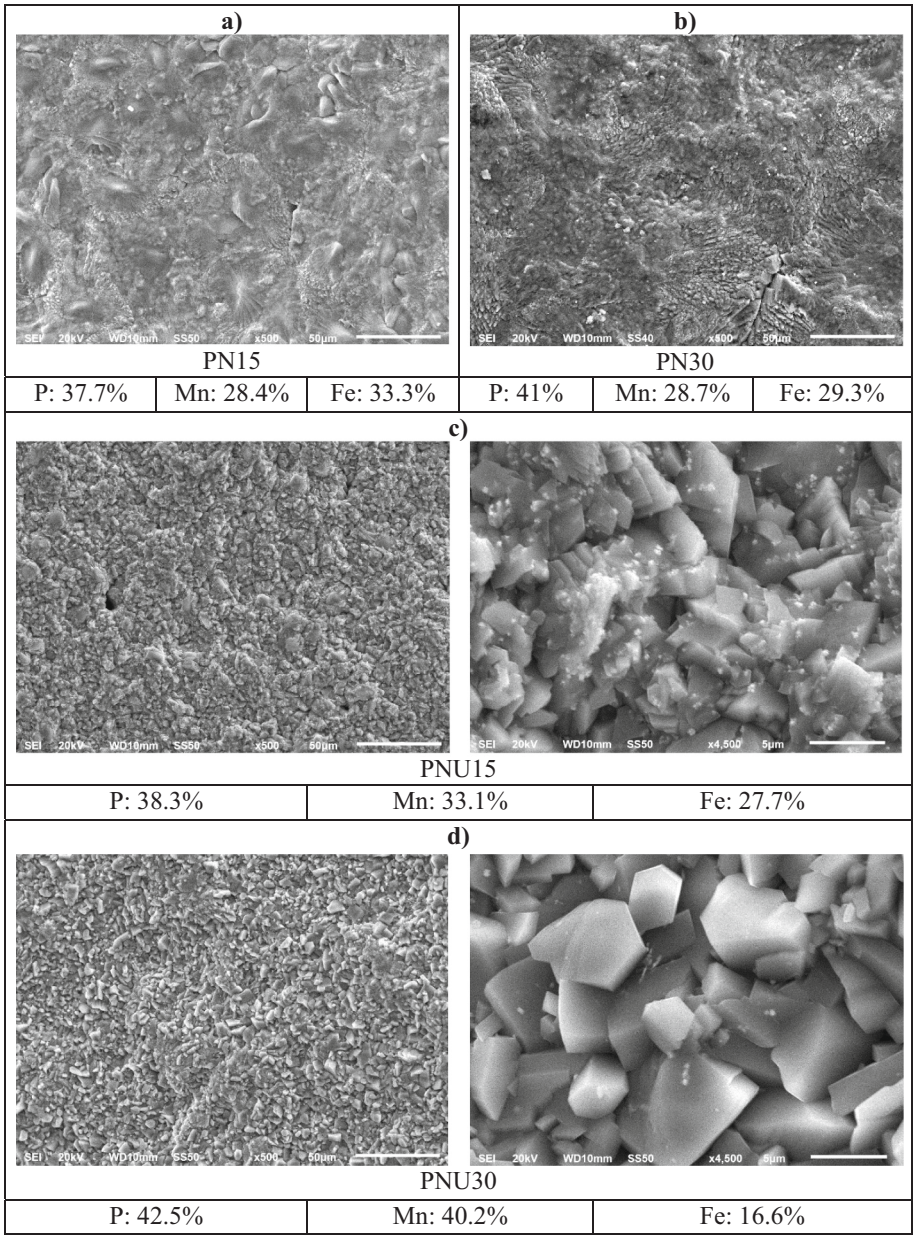

Fig. 5. SEM images for the phosphate films that were prepared in the bath with $Ni(NO_3)_2$ without stirring for, a) 15 min and b) 30 min; and under ultrasonic induced stirring for c) 15 min and d) 30 min. The chemical analysis as the atomic % is included.

electrolyte to the uncoated areas. Both increased immersion time (P30) and the use of stirring (PU15) assisted in the growth of more defective layers, and an increased portion of the substrate was uncovered, leading to the smaller R_s value that was obtained. The increased treatment in the stirred bath (PU30) reduces the electrolyte accessibility compared to PU15, which is consistent with the development of a more tortuous film, as described above.

The increase in the concentration of the activator promotes the formation of a layer with a slightly enhanced coating efficiency (P30 vs. PB30). No important change was obtained for the Z_1 time constant after the change in the activation stage so that a similar film resistivity was obtained. Both the R_m and R_s values decreased compared to the original activation solution, and, therefore, the change in the activation creates a less intricate film with a shorter conductive path.

3.2. Bath N (adding $Ni(NO_3)_2$): influence of immersion time and ultrasonic stirring

3.2.1. SEM/EDS characterisation

SEM images of the phosphate layers that were developed after adding $Ni(NO_3)_2$ to the bath are presented in Fig. 5. The influence of the phosphating time and the stirring bath is presented. In the absence of stirring, the film morphology is similar to that observed without Ni $(NO_3)_2$. Coarse crystals (some larger than 50 μm) arranged into thin layers were also developed, and they are a more recognisable characteristic of a film that was obtained after a longer immersion period. Adding $Ni(NO_3)_2$ promotes the growth of a layer with an increased Fe content [18], which was markedly greater than that of the shorter phosphating time. The P/Mn + Fe ratio decreased to 0.6 for the layer that developed after 15 min and to 0.7 for the layer that was prepared in 30 min. This means that the film was not uniquely composed of the expected hureaulite and that other compounds could have been developed. Additionally, the Fe/Mn ratio was greater than 1, whereas it was significantly lower for the layers grown in the original bath. Thus, adding nitrates supports the incorporation of Fe into the film due to their oxidising characteristic. The amount of the accelerator could be adjusted according to the requirements for the coating composition to match the desired performance.

The refinement produced by integration of ultrasonic stirring was also verified when the bath included $Ni(NO_3)_2$. Smaller crystals were detected in this case compared to the original stirred bath. The average crystal size was 2 μm, and it was measured for the film that developed after 15 min. The longer treatment seems to promote the formation of slightly larger crystals (approximately 5 μm). The Mn enrichment was more significant for the longer treatment, which is consistent with the above discussion on the effect of the ultrasonic vibration. However, the Fe/Mn ratio remains higher than that computed for the films that were developed in the absence of $Ni(NO_3)_2$ (Fig. 2c and d). The amount of Ni that was incorporated to these films was very low, and, although it is not included in the atomic percentage values, it corresponds to the difference to 100 % for each layer.

3.2.2. Coating weight and polarisation curves

Table 5 includes the values of the coating weights that were measured after removing the phosphate film from the substrate. A marked increase in the coating weight was obtained after incorporating the nitrate. The influence of the immersion period was also shown. An increase of 80 % and 115 % was calculated after immersion without Ni $(NO_3)_2$ for 15 and 30 min, respectively, compared with the values obtained for the stagnant bath. The influence of the NO_3^- ions as an accelerating agent was previously shown [1,8,18]. However, the combination with ultrasounds limits its ability to coat the mass. The effect of the ultrasound is better than changing the bath composition. The noticeable increase in the crystals' density due to the ultrasound restricts the expected film growth due to the nitrates. A direct correlation between the crystal size and the coating mass was shown (Table 5). Thus, an important decrease in the mass was obtained for the layers that were prepared using ultrasonic stirring and having the smallest crystals. Contrary to the growth that was obtained in the stirred bath without the accelerator, the coating growth almost stabilised after 15 min. Additionally, after the longer treatment, a slight reduction in the mass was obtained under this condition compared to the original stirred bath. The combined effect of both variables, adding the $Ni(NO_3)_2$, and ultrasound, modified the conclusions that were drawn when these variables are discussed separately. Thus, with $Ni(NO_3)_2$ and ultrasounds, the coating formed in 15 min is thicker than that formed in the original stirred bath, with no significant modifications after 30 min.

Table 5
Results corresponding to coating weights and current densities for the layers obtained in bath N. (*see the experimental conditions in Table 2).

Sample*	Coating weight (g/m^2)	i_{corr} ($\mu A/cm^2$)	E_{corr} ($mV_{vs.\ Hg/HgSO4}$)
PN15	23.9	3.47	−801
PN30	38.9	1.61	−784
PNU15	16.9	3.13	−762
PNU30	19.6	0.93	−744

The polarisation curves of the films that were developed in the bath with nitrates are presented in Fig. 6. The current density values along with the corrosion potential results are shown in Table 5. The shorter phosphating time in both the stagnant and stirred processes leads to the growth of a more porous layer (with a higher current density) than those developed in the original baths, even though the film was thicker (Table 3, P15 and PU15). A marked improvement was obtained after increasing the phosphating time to 30 min. Thus, the phosphate coating continues improving in the nitrate bath after the first 15 min. This enhancement correlates with the formation of a thicker film, which was more marked with the stagnant bath, and an improved covering, which was larger for the stirred bath. Thus, the growing effect of the accelerating agent is more evident for the stagnant bath. However, the extended immersion under ultrasonic stirring promotes the formation of a more compact deposit. The more anodic corrosion potential values recorded for the coated samples point to an enhanced corrosion performance as well.

Ultrasonic vibration in the bath with $Ni(NO_3)_2$ induces the formation of many crystals. After 15 min, there was not enough crystal development to create a dense film. The increase in the immersion time assists the crystal growth, which covers the substrate more efficiently. Because

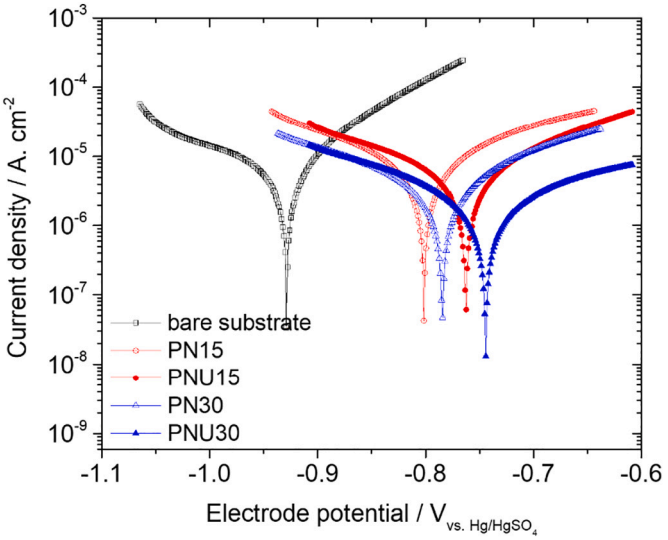

Fig. 6. Polarisation curves of the phosphate films that were prepared in the bath containing $Ni(NO_3)_2$.

there were no large changes in the mass, the width of the existing crystals increased but not the height, to fill any remaining uncoated space after a short immersion period. This suggestion is consistent with the improvement that was obtained in the corrosion performance, which indicates the development of a more compact film with the longer treatment. This type of development results in only a slight modification in the coating mass, but an enhanced covering efficiency was achieved.

3.2.3. Electrochemical impedance spectroscopy analysis

Fig. 7 shows the Nyquist plots corresponding to the layers that were developed in the bath that included $Ni(NO_3)_2$. The fitting parameters are presented in Table 6. Good correspondence with the corrosion current density was also obtained for the R_2 and C_2 values. The most corrosion-resistant film was developed after 30 min under stirring conditions, whereas both layers that were developed after 15 min showed the poorest corrosion performance.

The R_1C_1 time constant shows differences among the phosphate layers that were obtained after 15 and 30 min. The time constant is longer for the layers that were prepared after the shorter immersion, which suggests a slower charge transference at the film/electrolyte interface. This result indicates the development of less conductive films, which have higher R_m values.

A higher R_2 value was associated with a higher R_s value. The layers obtained after 30 min provide a more efficient covering than those prepared after 15 min, in both the still and the stirred bath. Thus, less of the substrate remained exposed to the electrolyte, resulting in higher values for R_s. The result obtained for the PNU30 film showed the best corrosion resistance (highest R_2), but the R_s value was particularly high compared to the other films. The low C_2 value obtained for this film also suggests a high degree of coating coverage that can help the ionic path to the metallic substrate to approach its percolation limit, where the associated resistance grows exponentially [40].

Comparing the data obtained from the layers that were prepared in the original bath is discussed next. Differences in the conduction ability can be observed, particularly among the layers that developed in the stagnant baths. Thus, the layers prepared in bath N had a longer time constant, which indicates poorer conductivity. The films prepared in the stagnant bath after 15 min differ significantly. The fitting values that were obtained suggest the development of a less tortuous film using

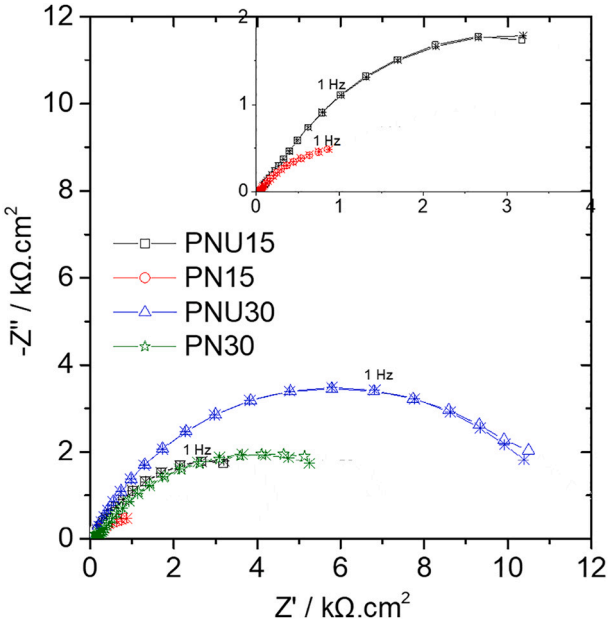

Fig. 7. Nyquist plots obtained in a 0.1 M Na_2SO_4 solution after growing the coatings in a bath with $Ni(NO_3)_2$. The fitted data are indicated with stars.

Table 6
Fitting parameters for phosphate layers that were prepared in bath N. The equivalent circuit that is presented in Fig. 1 was used for this fitting.

	R_m (kΩ. cm)	R_s (kΩ. cm)	R_1 (Ω. cm^3)	C_1 (mF. cm^{-3})	a_1	R_2 (kΩ. cm^2)	C_2 (μF. cm^{-2})	a_2
PN15	1410.3	31.1	2.9	535.9	0.5	16.5	27.9	0.8
PN30	163.9	47.2	12.2	40.2	0.6	33.9	9.9	0.7
PNU15	1266.1	29.7	4.9	284.3	0.7	13.5	44.3	0.7
PNU30	139.7	179.9	8.1	16.7	0.6	44.6	2.4	0.8

nitrates, because, although it is a less efficient layer, the R_m and R_s values were lower than those from the film that was obtained in the original bath. Thus, the accurate value for the phosphate electrical path in the P15 phosphate would cause a decrease in these parameters. After a longer immersion, bath N produced a denser film, and no significant modifications are expected in terms of the tortuosity. The low R_m and high R_s values that were obtained in bath N suggests the changes that were observed in the covering efficiency.

Bath N worsened the covering ability after the shorter immersion once the stirring was incorporated. A higher R_s value was obtained in this film (PNU15 vs. PU15) so greater tortuosity (or coating coverage) is expected. After phosphating for 30 min, a similar conclusion can be drawn. In this case, less marked changes in the covering level were identified so a more important modification in the tortuosity is expected (PNU30 vs PU30).

3.3. SEM cross-sectional analyses

The cross-sectional SEM micrographs and the EDS results are shown in Fig. 8. This discussion focuses on the influence of ultrasonic vibration, adding $Ni(NO_3)_2$, and modifying the activation for the coatings that were prepared after immersion for 30 min. The images show the formation of well-adhered films that are able to uniformly cover the rough metallic substrate.

The phosphate thicknesses can be evaluated from the SEM cross-sectional images and EDS profiles. The measured thicknesses are not uniform, although, when averaged, they are consistent with the trend in the coating masses that were already discussed. These thickness values are not as realistic as the coating mass because they were taken at localised positions in the film. However, a decrease in the thickness was verified in the baths with and without the $Ni(NO_3)_2$ due to the effect of the ultrasound. Adding $Ni(NO_3)_2$, without vibrations, produced a thicker film, whereas the change in the activator did not provide large alterations.

The concentration profiles (atomic percentages) of Fe and Mn are also presented in Fig. 8. These scans were performed along the lines that are indicated on the corresponding SEM images. A lower Fe content was observed for the phosphate prepared with ultrasound in the original bath. The Mn distribution was also modified. The ultrasound developed a film where the Mn was practically uniformly distributed throughout the film thickness, whereas without stirring, the outer portion was preferentially enriched in this element. With stirring, approximately 90 % of the total thickness in most of the film had an amount of Mn that was greater than that of Fe. However, for the film that was grown under still conditions, this percentage was reduced to about 50 %. The P30 film contained almost 22 % of Mn, and the Fe/Mn ratio was greater than 1.

After activation, in the more concentrated solution, the phosphate contained a similar percentage of both elements in the middle and outer portions, which corresponded to 76 % of the total thickness, and a higher Fe/Mn was verified. The amount of Mn was not greater than the Fe percentage in any portion. However, in the inner portion, approximately 24 % of the total thickness, the Fe/Mn ratio was much greater than 1.

The coating prepared with $Ni(NO_3)_2$ also contained the same amount of each element, although it was enriched in Fe in the inner and middle

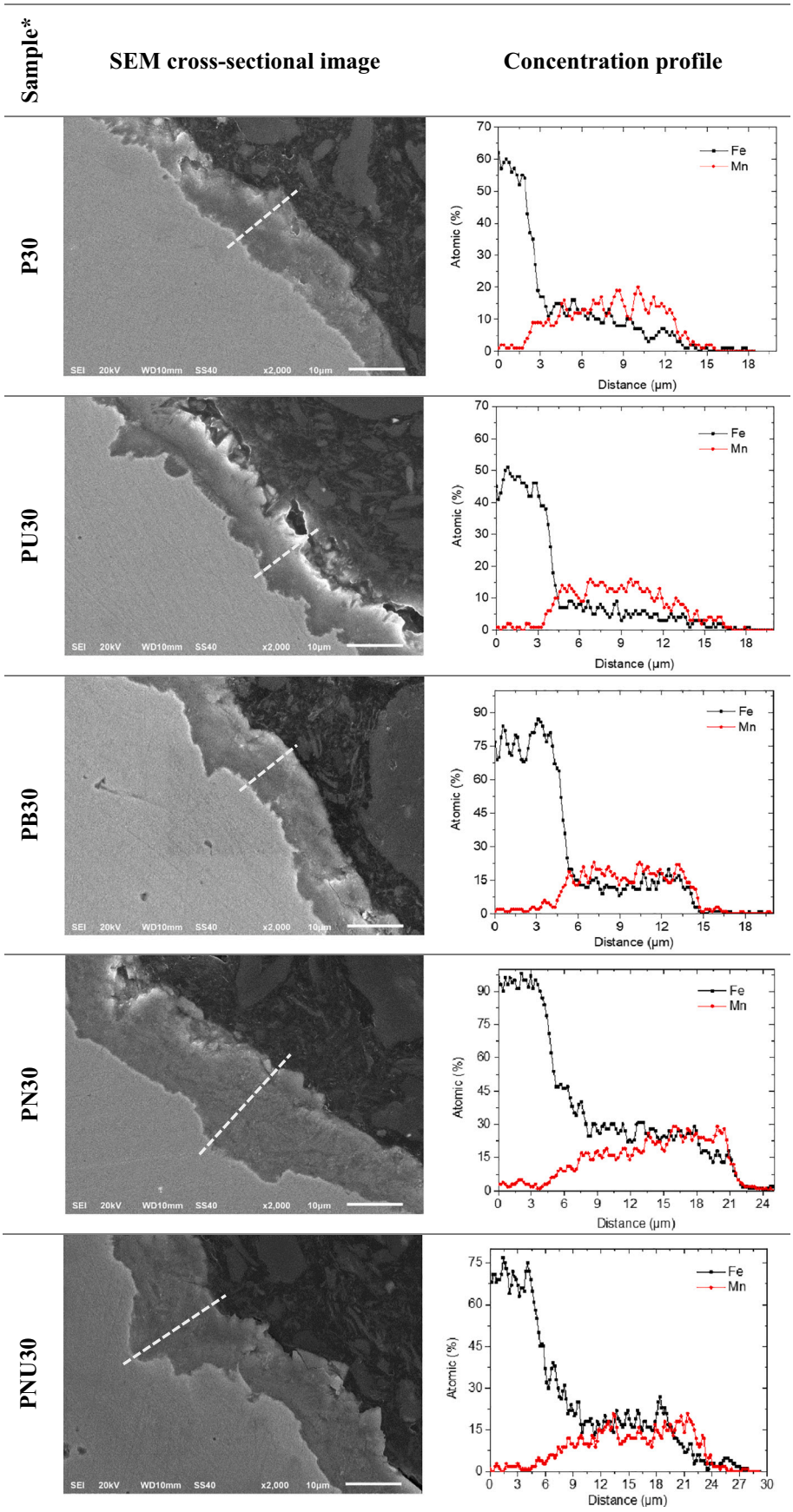

Fig. 8. SEM cross sectional images of the films that developed after 30 min (from left to right: substrate, phosphate film and mounting resin) and corresponding concentration profiles (*see Table 2 for details).

fragments. This corresponds to almost 55 % of the total thickness, and it is a thicker portion than computed for the original bath (24 %). At these positions, the Fe level was significantly higher than the amount obtained in the films that were prepared in the original bath. Ultrasonic vibration with nitrates did not produce large changes in the distribution of Fe and Mn, although the inner fraction with a high Fe content was thinner, corresponding to approximately 28 % of the total thickness. Moreover, the outermost area retains a higher Mn/Fe ratio. A thicker portion, approximately 52 % of the total thickness, was also measured in the middle position where the amount of Fe was almost the same as the amount of Mn.

3.4. Pin-on-disk results

The purpose of this section is to understand the influence of the characteristics of the phosphate films, including the morphology, structure, chemical composition, and mass, on the wear resistance. Fig. 9 shows the variation of the friction coefficients that were recorded with the sliding distance. The coefficients of friction (COF) of the uncoated and coated specimens were measured without lubricant. The important noise reflected in the results could be related to this experimental condition [41].

The friction coefficient for the bare substrate stabilised at about 0.55 after a short period, where it sharply increased. At short distances, the phosphated samples retained a low value for the coefficient of friction suggesting the development of wear-resistant films, as expected [38,42]. For some specimens, an initial run-in period, that was attributed to changes in the surface roughness [41], can be observed before an almost steady-state value is reached. The friction coefficient then increases in a fairly sharp manner and finally stabilises at a higher value that is associated with complete phosphate elimination. This last period corresponds to the decrease in the phosphate layers due to the gradual elimination of the film until the loaded pin interacts directly with the metallic substrate [43].

To quantitatively conclude differences among the prepared films, several parameters have been determined. An average friction coefficient was obtained from the steady state condition that was observed at short distances. The onset of damage was determined as the distance where the friction coefficient increases more markedly, which was taken from the intersection of the two linear parts of the curve, as shown in Fig. 6c [43]. The two linear parts were fitted, and the distance at which the friction coefficients intersect was computed. The computed values, along with the averaged friction coefficients, are presented in Table 7.

No results are presented for the PU15 film because, due to its reduced thickness, it showed no improved performance compared to the bare substrate (under the used wear condition).

The damage onset distances were first compared. The layer that developed after 15 min in the stagnant bath behaves better than the layer that was obtained after 30 min. Because both films had a similar thickness and an analogous surface appearance and chemical composition, a hidden factor could contribute to the poorer wear resistance. The above-mentioned modification relating to the growth of a more tortuous film could be a decisive circumstance. Thus, the thin film growth in the last stage of the phosphating process (between 15 and 30 min) creates an intricate structure that is more susceptible to damage caused by friction.

Modifications induced due to the incorporation of the ultrasonic vibration in the original bath (PU30 vs. P30), which is mostly associated with crystal refinement, Mn enrichment, compactness, and tortuosity, significantly enhance the wear performance. A reduction in crystal size was also produced after modifying the activation solution (phosphate PB30), but a higher Fe content was found, along with less tortuosity and almost the same covering efficiency. Both films, which were produced using ultrasound and that were obtained after increasing the activator concentration, provide improved behaviour. Thus, the crystal size, which is the only common circumstance in both films, has a more important impact on the phosphate wear resistance, at least in terms of

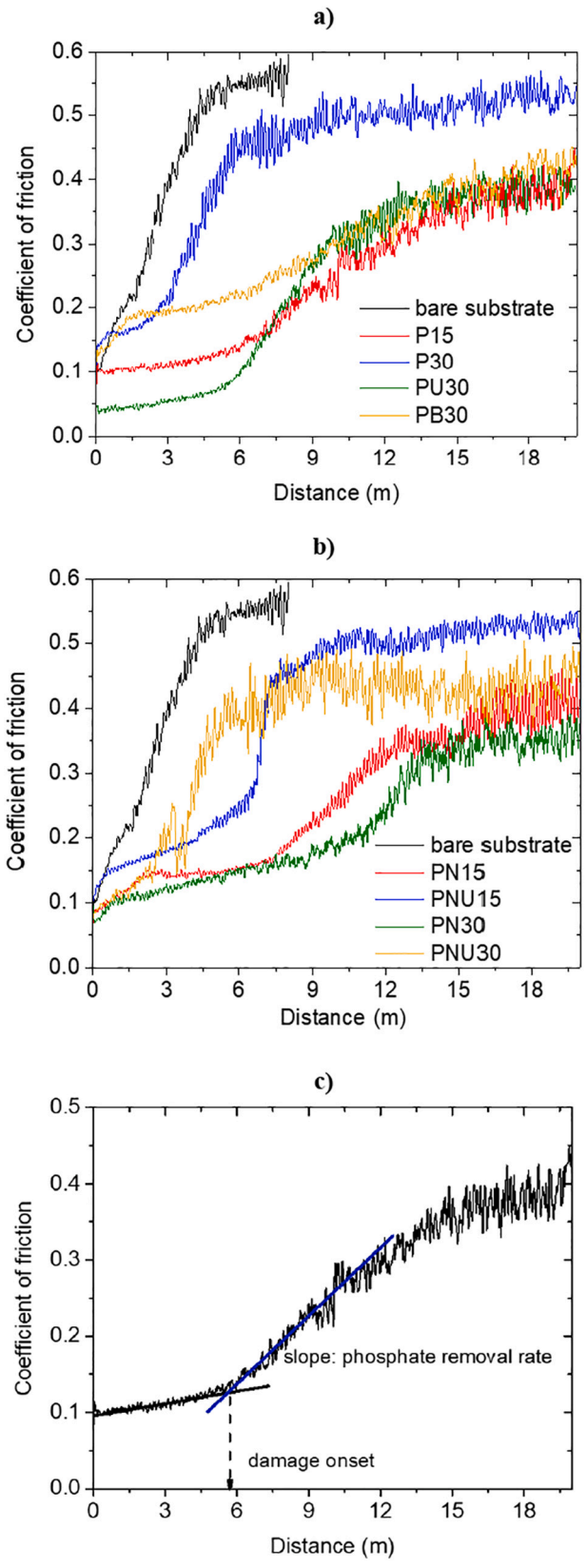

Fig. 9. Variation in the coefficient of friction as a function of the sliding distance for the layers prepared in a) bath A and b) bath N (with $Ni(NO_3)_2$). c) Graphic representation to determine the damage onset (given as the distance) and the removal rate (given as the variation of the coefficient of friction [COF] with the sliding distance).

Table 7
Friction coefficient values, damage onset, and removal rate determined from the pin-on-disk tests.

	Friction coefficient	Damage onset (m)	Removal rate (m^{-1})
P15	0.11	5.10	0.0259
P30	0.17	2.73	0.0822
PU15	–	–	–
PU30	0.05	5.46	0.0558
PB30	0.19	5.29	0.0186
PN15	0.15	6.78	0.0324
PN30	0.14	10.27	0.0359
PNU15	0.18	6.06	0.1306
PNU30	0.12	2.59	0.0824

degradation onset, whereas the other properties could have a direct effect on parameters such as the friction coefficient or the removal rate, which will be discussed later.

A marked change was also observed after adding $Ni(NO_3)_2$ to the phosphating bath. The time to onset of the film damage was the largest, which is likely related to the greater coating mass that was developed with this compound. An improvement was obtained at 30 min compared to 15 min due to the increased immersion period and the coating mass [44]. The percentage of improvement was slightly less than what would be expected due to the increase in thickness. This observation means that the innermost layer, which developed in the first minutes of immersion, is mainly responsible for the improved wear performance. The outer portion seems to be more easily removed under frictional forces.

The film prepared under ultrasonic vibration in this modified bath shows a degradation at shorter distances, which was greater for the coating obtained after 30 min, despite the observed crystal size refinement. An explanation could be the thinner coating compared to the film obtained in the same bath but under stagnant conditions. Thus, the increased crystal density could improve the wear behaviour, but due to the formation of a thinner layer, the expected benefit is negated.

The deterioration was particularly significant for the PNU30 film. In addition to the crystal refinement, this film had the smallest uncovered area and the most compactness. This quality could have a more important effect on the poor wear performance that was observed because the other characteristics had already been verified using the PNU15 film, which behaved comparably better. The structure that was developed for the PNU30 film showed weaker bonding among the many crystals and was more easily detached from the substrate during the sliding process. The individual crystals could be removed from the film during the friction test, producing a more intense erosive effect and assisting with the faster film loss.

The Fe/Mn ratio that was determined from the EDS analysis (Sections 3.1.1 and 3.2.1) seems to have an effect on the coefficient of friction values. Thus, the lowest friction coefficients were obtained for the P15, PU30, and PNU30 layers where the Fe/Mn ratio was below 0.5.

In Fig. 9c, the slope obtained from the variation of the coefficient of friction at the intermediate stage, after the initial steady condition and before the complete removal of phosphate, may suggest some differences in the coating's resistance to being removed, such us how fast the coating is damaged due to the frictional force.

Extending the immersion period in the original stagnant bath (A) produces a weaker film that is more quickly removed (P30 vs. P15). The difference regarding tortuosity may explain this worsened performance. Thus, tortuosity decreases both the damage onset and the film removal rate; the other phosphate properties are almost the same (appearance, crystal size, and composition).

The smaller crystal size developed under stirring conditions after 30 min (PU30 vs. P30), which delays the removal period. A longer film removal period is required for the layer that developed after using a more concentrated activation solution (PB30), where the crystal refinement was less important. Small crystals expand the wear period, but below a critical crystal size, the film is more rapidly degraded, which agrees with Hivart et al. [43].

Another common factor among the films with the lowest removal rate (PB30, PN15, and PN30) was the high Fe/Mn ratio, which was greater than 1 in all of the films. However, the films with the shortest removal period had a greater Mn content and smaller crystals. The layer that had the smallest crystals and a slightly lower Fe/Mn ratio (0.9) was PNU15 (Fig. 5c), which was rapidly removed. The layers with slightly larger crystals (PNU30 and PU30) along with a very low Fe/Mn ratio (under 0.4) were also easily detached. A tortuous structure had also been observed in these two layers, which is a characteristic that contributes to poorer wear resistance.

4. Conclusions

The main concluding remarks of the present study are listed below.

1) Incorporating accelerators into the phosphating bath promotes the growth of thicker layers with a higher Fe content. Stirring the bath helps to reduce the Fe/Mn ratio and decreases the coating mass (more substantially in the bath with the largest amount of accelerator).
2) Ultrasonic vibration develops films with smaller crystal size, which is more noticeable when the bath contains $Ni(NO_3)_2$. Previous activation also plays a role in the crystal density, but a less marked influence was identified.
3) The electrochemical analysis allowed the determination of differences in the covering efficiency, film resistivity, and growth structure. Crystal size seems to be the most relevant parameter to enhance the corrosion performance of the coated specimens rather than the coating mass. In addition, a reduction in the Fe content of the phosphate films along with a more intricate internal structure was detected in the films with the greatest corrosion resistance.
4) The most important factor influencing the wear performance was the coating mass. The layers that developed in the bath with $Ni(NO_3)_2$ provided the longest period before damage onset during friction. The crystal refinement also improved the wear behaviour in terms of the coefficient of friction, but even the phosphate layers that are composed of smaller crystals are more rapidly removed from the substrate. A tortuous phosphate structure decreases the performance under frictional forces.

CRediT authorship contribution statement

Sheila Silva-Fernández: Conceptualization, Data curation, Formal analysis, Investigation, Methodology, Validation, Writing – review & editing. **Belén Díaz:** Conceptualization, Data curation, Formal analysis, Methodology, Supervision, Writing – original draft, Writing – review & editing, Validation. **Raúl Figueroa:** Conceptualization, Data curation, Formal analysis, Writing – review & editing, Validation. **X. Ramón Nóvoa:** Conceptualization, Funding acquisition, Project administration, Supervision, Validation, Writing – review & editing. **Carmen Pérez:** Conceptualization, Formal analysis, Methodology, Supervision, Validation, Writing – review & editing.

Declaration of competing interest

The authors declare that they have no known competing financial interests or personal relationships that could have appeared to influence the work reported in this paper.

Data availability

The raw and/or processed data required to reproduce these findings are available from the corresponding authors upon request.

Acknowledgments

ArcelorMittal is acknowledged for supplying the high-strength steel rods. We also thank Ismael Vieito from Galcore S.L. for the technical assistance.

References

[1] W. Rausch, The Phosphating of Metals, Finishing Publications Ltd., 1990.
[2] X.B. Chen, X. Zhou, T.B. Abbott, M.A. Easton, N. Birbilis, Double-layered manganese phosphate conversion coating on magnesium alloy AZ91D: insights into coating formation, growth and corrosion resistance, Surf. Coatings Technol. 217 (2013) 147–155, https://doi.org/10.1016/j.surfcoat.2012.12.005.
[3] S. Pommiers, J.Ô. Frayret, A. Castetbon, M. Potin-Gautier, Alternative conversion coatings to chromate for the protection of magnesium alloys, Corros. Sci. 84 (2014) 135–146, https://doi.org/10.1016/j.corsci.2014.03.021.
[4] S. Zhang, L. Liu, Q. Lei, T. Zhang, J. Bing, J. Dong, A nano-CeO2/Zn–Mn composite conversion coatings on AZ91D magnesium alloy surface of corrosion resistance research, Coatings 13 (2023), https://doi.org/10.3390/coatings13 050929.
[5] I. Milošev, G.S. Frankel, Review—conversion coatings based on zirconium and/or titanium, J. Electrochem. Soc. 165 (2018), https://doi.org/10.1149/2.0371803jes. C127–C144.
[6] B.L. Ellis, W.R.M. Makahnouk, Y. Makimura, K. Toghill, L.F. Nazar, A multifunctional 3.5V iron-based phosphate cathode for rechargeable batteries, Nat. Mater. 6 (2007) 749–753, https://doi.org/10.1038/nmat2007.
[7] K.B. Gandrud, A. Pettersen, O. Nilsen, H. Fjellvåg, High-performing iron phosphate for enhanced lithium ion solid state batteries as grown by atomic layer deposition, J. Mater. Chem. A 1 (2013) 9054–9059, https://doi.org/10.1039/c3ta11550j.
[8] L. Fang, L.B. Xie, J. Hu, Y. Li, W.T. Zhang, Study on the growth and corrosion resistance of manganese phosphate coatings on 30CrMnMoTi alloy steel, Phys. Procedia 18 (2011) 227–233, https://doi.org/10.1016/j.phpro.2011.06.086.
[9] J. Duszczyk, K. Siuzdak, T. Klimczuk, J. Strychalska-Nowak, A. Zaleska-Medynska, Manganese phosphatizing coatings: the effects of preparation conditions on surface properties, Materials (Basel). 11 (2018) doi:10.3390/ma11122585.
[10] L. Zang, Y. Chen, Y. Wu, Y. Zheng, H. Chen, D. You, L. Li, J. Li, Comparative tribological and friction behaviors of oil-lubricated manganese phosphate conversion coatings with different crystal sizes on AISI 52100 steel, Wear 458–459 (2020), 203427, https://doi.org/10.1016/j.wear.2020.203427.
[11] C. Galvan-Reyes, J.C. Fuentes-Aceituno, A. Salinas-Rodríguez, The role of alkalizing agent on the manganese phosphating of a high strength steel part 1: the individual effect of NaOH and NH4OH, Surf. Coatings Technol. 291 (2016) 179–188, https://doi.org/10.1016/j.surfcoat.2016.02.012.
[12] L. Guo, Q. Huang, C. Zhang, J. Wang, G. Shen, C. Ban, L. Guo, Study on the formation of Mn-P coatings with significant corrosion resistance on Q235 carbon steels by adjusting the ratio of phosphorus to manganese, Corros. Sci. 178 (2021), 108960, https://doi.org/10.1016/j.corsci.2020.108960.
[13] M. Padma, S. Shanmugam, K. Ravichandran, Sodium silicate assisted manganese phosphate chemical conversion coating on D2 steel at various concentration, Surfaces and Interfaces. 20 (2020), 100547, https://doi.org/10.1016/j.surfin.2020.100547.
[14] S. Shanmugam, K. Ravichandran, T.S.N. Sankara Narayanan, M. Marappan, Development of permanganate assisted manganese phosphate coating on mild steel, Corros. Eng. Sci. Technol. 49 (2014) 719–726, https://doi.org/10.1179/1743278214Y. 0000000169.
[15] J. Duszczyk, K. Siuzdak, T. Klimczuk, J. Strychalska-Nowak, A. Zaleska-Medynska, Modified manganese phosphate conversion coating on low-carbon steel, Materials (Basel). 13 (2020), https://doi.org/10.3390/ma13061416.
[16] F. Pastorek, K. Borko, S. Fintová, D. Kajánek, B. Hadzima, Effect of surface pretreatment on quality and electrochemical corrosion properties of manganese phosphate on S355J2 HSLA steel, Coatings 6 (2016) 46, https://doi.org/10.3390/coatings 6040046.
[17] Z. Panossian, Phosphating of steel for cold forming processes, in: Q.J. Wang, Y. W. Chung (Eds.), Encycl. Tribollogy, 2013, https://doi.org/10.1007/978-0-387-92897-5_1187.
[18] T.S.N.S. Narayanan, Surface pretreatment by phosphate conversion coatings - a review, Rev. Adv. Mater. Sci. 9 (2005) 130–177.
[19] Y. Xie, M. Chen, D. Xie, L. Zhong, X. Zhang, A fast, low temperature zinc phosphate coating on steel accelerated by graphene oxide, Corros. Sci. 128 (2017) 1–8, https://doi.org/10.1016/j.corsci.2017.08.033.
[20] H. Huang, H. Wang, Y. Xie, D. Dong, X. Jiang, X. Zhang, Incorporation of boron nitride nanosheets in zinc phosphate coatings on mild steel to enhance corrosion resistance, Surf. Coatings Technol. 374 (2019) 935–943, doi:10.10.16/j.surfcoat.2019.06.082.
[21] Y. Tian, H. Huang, H. Wang, Y. Xie, X. Sheng, L. Zhong, X. Zhang, Accelerated formation of zinc phosphate coatings with enhanced corrosion resistance on carbon steel by introducing α-zirconium phosphate, J. Alloys Compd. 831 (2020), 154906, https://doi.org/10.1016/j.jallcom.2020.154906.
[22] Y. Tian, W. Qiu, Y. Xie, H. Huang, J. Hu, L. Zhong, X. Jiang, X. Zhang, Melatonin as an accelerating agent for phosphate chemical conversion coatings on mild steel with enhanced corrosion resistance, J. Electrochem. Soc. 167 (2020), 101505, https://doi.org/10.1149/1945-7111/ab9b0f.
[23] W. Wang, Y. Tian, A. Ke, H. Huang, H. Shen, X. Zhang, Enalapril maleate as a green accelerator for zinc phosphating coating on low-carbon steel, J. Ind. Eng. Chem. 120 (2023) 477–486, https://doi.org/10.1016/j.jiec.2022.12.056.
[24] J.K. Yang, J.G. Kim, J.S. Chun, A study of the effect of ultrasonics on manganese phosphating of steel, Thin Solid Films 101 (1983) 193–200, https://doi.org/10.1016/0040-6090(83)90245-6.
[25] X. Sun, M. Liu, J. Song, Y. Xu, Corrosion behaviors of hybrid ultrasonic phosphating coatings on carbon steel in simulated 150 °C hot-dry-rock fluids, Geothermics 86 (2020), 101807, https://doi.org/10.1016/j.geothermics.2020.101807.
[26] D. Weng, P. Jokiel, A. Uebleis, H. Boehni, Corrosion and protection characteristics of zinc and manganese phosphate coatings, Surf. Coatings Technol. 88 (1997) 147–156, https://doi.org/10.1016/S0257-8972(96)02860-5.
[27] B. Díaz, L. Freire, M. Mojío, X.R. Nóvoa, Optimization of conversion coatings based on zinc phosphate on high strength steels, with enhanced barrier properties, J. Electroanal. Chem. 737 (2015) 174–183, https://doi.org/10.1016/j.jelechem.2014.06.035.
[28] B. Díaz, L. Freire, M. Mojío, X.R. Nóvoa, Effect of carbon on the corrosion and wear performance of Zn-phosphate layers, Electrochim. Acta 202 (2016) 299–309, https://doi.org/10.1016/j.electacta.2015.12.083.
[29] J.R. Park, D.D. Macdonald, Impedance studies of the growth of porous magnetite films on carbon steel in high temperature aqueous systems, Corros. Sci. 23 (1983) 295–315, https://doi.org/10.1016/0010-938X(83)90063-X.
[30] B. Guitián, S. Lascaud, X.R. Nóvoa, L. Ribeaucourt, E. Vidal, On the growth of nanostructured iron hydroxy-fluorides for Li-ion batteries, J. Power Sources 241 (2013) 567–571, https://doi.org/10.1016/j.jpowsour.2013.04.145.
[31] M. Sheng, C. Wang, Q. Zhong, Y. Wei, Y. Wang, Ultrasonic irradiation and its application for improving the corrosion resistance of phosphate coatings on aluminum alloys, Ultrason. Sonochem. 17 (2010) 21–25, https://doi.org/10.1016/j.ultsonch. 2009.07.006.
[32] C.H.S.B. Teixeira, E.A. Alvarenga, W.L. Vasconcelos, V.F.C. Lins, Effect of porosity of phosphate coating on corrosion resistance of galvanized and phosphated steels part I: measurement of porosity of phosphate, Mater. Corros. 62 (2011) 771–777, https://doi.org/10.1002/maco.200905503.
[33] M. Wolpers, J. Angeli, Activation of galvanized steel surfaces before zinc phosphating - XPS and GDOES investigations, Appl. Surf. Sci. 179 (2001) 281–291, https://doi.org/10.1016/S0169-4332(01)00296-3.
[34] K. Abdalla, A. Rahmat, A. Azizan, Influence of activation treatment with nickel acetate on the zinc phosphate coating formation and corrosion resistance, Mater. Corros. 65 (2014) 977–981, https://doi.org/10.1002/maco.201307009.
[35] P. Tanguy, C. Allély, D. Dragoe, V. Sefl, J. Stoulil, P. Volovitch, On the effect of multiphase microstructure of ZnAlMg substrate on the Ti-based activation and phosphate conversion coating distribution, Surf. Coatings Technol. 369 (2019) 165–174, https://doi.org/10.1016/j.surfcoat.2019.04.050.
[36] C.M. Wang, H.C. Liau, W.T. Tsai, Effect of heat treatment on the microstructure and electrochemical behavior of manganese phosphate coating, Mater. Chem. Phys. 102 (2007) 207–213, https://doi.org/10.1016/j.matchemphys.2006.12.012.
[37] P.E. Tegehall, The mechanism of chemical activation with titanium phosphate colloids in the formation of zinc phosphate conversion coatings, Colloids Surf. 49 (1990) 373–383, https://doi.org/10.1016/0166-6622(90)80118-N.
[38] S. Azhaarudeen, A.A.M. Faruck, A. Nevosad, Tribological behaviour and wear mechanisms of manganese phosphate coatings under dry reciprocating sliding contact conditions, Tribol. Int. 122 (2018) 189–199, https://doi.org/10.1016/j.triboint.2018. 02.043.
[39] X. Zhang, G. Yong Xiao, C. Cong Jiang, B. Liu, N. Bo Li, R. Fu Zhu, Y. Peng Lu, Influence of process parameters on microstructure and corrosion properties of hopeite coating on stainless steel, Corros. Sci. 94 (2015) 428–437, https://doi.org/10.1016/j. corsci.2015.02.021.
[40] L. Jiang, Z. Liu, Y. Yu, X. Ben, The effect of graphene on the conductivity of magnesium sulfate cement, Construct. Build Mater. 312 (2021), 125342 doi:10.10.16/j.conbuildmat.2021.125342.
[41] P.J. Blau, Friction Science and Technology: From Concepts to Applications, Second Edition, CRC Press, Taylor & Francis Group, 2008.
[42] A. Kozlowski, W. Czechowski, Wear resistance of manganese phosphate coatings, Electrodepos. Surf. Treat. 3 (1975) 55–63, https://doi.org/10.1016/0300-941 6(75)90011-5.
[43] P. Hivart, B. Hauw, J.P. Bricout, J. Oudin, Seizure behaviour of manganese phosphate coatings according to the process conditions, Tribol. Int. 30 (1997) 561–570, https://doi.org/10.1016/S0301-679X(97)00019-4.
[44] A. Kozlowski, Dry friction of manganese phosphate coatings on steel and cast iron, Electrodepos. Surf. Treat. 2 (1973) 109–122.